Chapter 2

Fundamentals of Radiative Transfer

2.1 The Radiative Transfer Equation

When electromagnetic radiation passes through matter, they interact. Radiation is attenuated by matter absorbing photons as well as scattering photons out of their straight path. Extinction is defined as the sum of attenuating absorption and scattering. It can be described mathematically by the extinction coefficient

$$\beta_\mathrm{e} \;=\; \beta_\mathrm{a} + \beta_\mathrm{s} \tag{2.1}$$

where β_a is the absorption coefficient and β_s the scattering coefficient, with dimension [length^{-1}], respectively. Following from that, the change in the amount of radiation along its path due to extinction can be described by

$$\frac{\mathrm{d}I}{\mathrm{d}s} \;=\; -\,\beta_\mathrm{e}\, I \tag{2.2}$$

where I denotes the monochromatic radiance or intensity, the energy per unit area, unit solid angle, and spectral unit of unit [W/(m^2 sr cm^{-1})]. Integrating Eq. (2.2) yields Beer's law, sometimes also referred to as the Lambert-Bouguer law

$$I(s) \;=\; I(0)\, e^{-\int_0^s \beta_\mathrm{e}\,\mathrm{d}s'}, \tag{2.3}$$

describing the decrease in intensity when passing a distance s through an extinction medium. Introducing optical depth or optical thickness τ of the medium along a path by

$$\tau \;=\; \int \beta_\mathrm{e}\,\mathrm{d}s, \tag{2.4}$$

transmission $\mathcal{T}$ can be defined by

$$\mathcal{T} \;=\; e^{-\tau}. \tag{2.5}$$

For reasons of energy conservation, attenuation has to be balanced by sources of radiation. Including a term J, that describes the sources of radiation, into Eq. (2.2) leads to the differential radiative transfer equation (RTE)

$$\frac{\mathrm{d}I}{\beta_\mathrm{e}\,\mathrm{d}s} \;=\; \frac{\mathrm{d}I}{\mathrm{d}\tau} \;=\; -\,I + J. \tag{2.6}$$

Correspondingly, the integral form of the RTE is given by

$$I(\tau) \;=\; I(0)\, e^{-\tau} + \int_0^{\tau} J(\tau')\, e^{-\tau'} \mathrm{d}\tau'. \tag{2.7}$$

Setting source term J to $J = B(T)$, where B denotes the Planck function, which represents the thermal emission of a blackbody at temperature T, Eq. (2.7) can be rewritten as the so-called Schwarzschild equation:

$$I(\tau) \;=\; I(0)\, e^{-\tau} + \int_0^{\tau} B(T(\tau'))\, e^{-\tau'} \mathrm{d}\tau'. \tag{2.8}$$

The monochromatic Planck function can be expressed as

$$B_\nu(T) \;=\; \frac{2h\nu^3 c^2}{e^{h\nu c/kT} - 1} \tag{2.9}$$

with ν being the wavenumber, c the speed of light, k and h denoting Boltzmann's and Planck's constant, respectively.[1]

While a blackbody absorbs all incident radiation and emits according to Planck's function, non-blackbody matter absorbs and emits only a fractional amount of it. Employing Kirchhoff's law, which states that in case of local thermodynamic equilibrium (LTE) absorptivity equals emissivity ($\alpha = \varepsilon$), leads to the thermal emission source term

$$J_\mathrm{B} \;=\; \frac{\beta_\mathrm{a}}{\beta_\mathrm{e}}\, B(T). \tag{2.10}$$

Complementary to attenuation by scattering out of a path, scattering into a path is considered as a source of radiation. The scattering source term

$$J_\mathrm{S}(\mathbf{\Omega}) \;=\; \frac{\beta_\mathrm{s}}{\beta_\mathrm{e}} \frac{1}{4\pi} \int_0^{4\pi} P(\mathbf{\Omega}, \mathbf{\Omega'})\, I(\mathbf{\Omega'})\, \mathrm{d}\Omega' \tag{2.11}$$

comprises radiation incident from all directions $\mathbf{\Omega'}$ scattered into the direction of interest $\mathbf{\Omega}$. While the scattering coefficient β_s accounts for the scattered fraction of radiation, the phase function P can be interpreted as the probability of incident radiation being scattered from direction $\mathbf{\Omega'}$ into direction $\mathbf{\Omega}$ with

$$\frac{1}{4\pi} \int_0^{4\pi} P(\mathbf{\Omega}, \mathbf{\Omega'})\, \mathrm{d}\Omega' \;=\; 1. \tag{2.12}$$

From Eq. (2.11) it has to be noted, that the calculation of the scattering source term requires the knowledge of the incident radiation field $I(\mathbf{\Omega'})$.

It is common to separate the scattering source term J_S into a term J_MS resulting from multiple scattered radiation and J_SS originating from single scattering of direct radiation from

[1] Subscript ν refers to the spectral dependency of monochromatic emission, that might as well be described in terms of wavelength λ and frequency $\tilde{\nu}$, with $1/\lambda = \nu = \tilde{\nu}/c$. Unless otherwise noted, the radiative quantities throughout this chapter are monochromatic, spectrally dependent quantities. Nevertheless, the subscript is omitted for reasons of better readability.

a beam source, e.g. the sun. In this case the multiple scattering source term J_{MS} is given by Eq. (2.11), with $I(\mathbf{\Omega}')$ representing the incident diffuse radiation field. The single scattering source term is described by

$$J_{\mathrm{SS}}(\mathbf{\Omega}') \;=\; \frac{\beta_{\mathrm{s}}}{\beta_{\mathrm{e}}}\,\frac{1}{4\pi}\,P(\mathbf{\Omega},\mathbf{\Omega}_{\odot})\,F_{\odot}\,\mathcal{T}_{\odot} \tag{2.13}$$

where $F_{\odot}$ denotes the extra-terrestrial solar irradiance and $\mathcal{T}_{\odot} = e^{-\tau_{\odot}}$ is the transmission along the path of the direct beam through the atmosphere from the top to the point of scattering. In summary, for source term J applies

$$J \;=\; J_{\mathrm{B}} + J_{\mathrm{SS}} + J_{\mathrm{MS}}. \tag{2.14}$$

In the course of this work, radiation will only be discussed in terms of scalar intensity. A complete description of interaction between matter and radiation is only possible, when polarization is considered and radiation is described by the four components (I,Q,U,V) of the Stokes vector. However, scalar radiative transfer is usually a good approximation to most tasks in radiative transfer modeling and atmospheric remote sensing.

2.2 Radiative Transfer of Solar and Terrestrial Radiation

As indicated in section 2.1, the sources of radiation may be separated with respect to origin, spatial and spectral behavior. The RTE can be simplified by neglecting certain source terms, when a distinction is drawn between solar and terrestrial radiation. Both are based on emission of electromagnetic radiation according to Planck's function, given by Eq. (2.9). The sun, with a surface temperature of $\approx 5800\,\mathrm{K}$, emits radiation with a maximum in the region of visible light. Terrestrial radiation results from a mean temperature of $\approx 300\,\mathrm{K}$ of the Earth-atmosphere system and, according to that, shows a maximum in the thermal infrared (TIR) around $10\,\mu\mathrm{m}$ (see Fig. 2.1).[2]

The sun, located far outside the Earth-atmosphere system, acts as a beam source. That means, radiation from the sun enters the system at the upper boundary, from top of atmosphere (TOA), out of an infinitesimal narrow solid angle. Therefore, sun light is taken for a bundle of parallel rays, emerging from a discrete direction. Except for this direct beam direction, solar radiation only contributes to the radiation field after being scattered. Few scattering occurs, when absorption is dominant and radiation from the sun is not able to penetrate the atmosphere. In case of weak scattering, the light is transmitted, but not spread into other directions than that of the direct beam. Thus, sun light is the driving source when scattering is strong, which is generally restricted to the shortwave spectral region from UV to NIR, in particular to the atmospheric window region of the VIS. Due to low scattering and dominant absorption, solar radiation has almost no relevance at wavelengths longer than $4\,\mu\mathrm{m}$.

From Fig. 2.1 it becomes evident, that terrestrial radiation is negligible at wavenumbers higher than approximately 4000 cm^{-1}, i.e. at wavelengths shorter than $2.5\,\mu\mathrm{m}$. Furthermore,

[2] The spectral regions will be denoted as follows: ultraviolet (UV) $0.3-0.4\,\mu\mathrm{m}$, visible (VIS) $0.4-0.7\,\mu\mathrm{m}$, near infrared (NIR) $0.7-3\,\mu\mathrm{m}$, thermal infrared (TIR) $3-40\,\mu\mathrm{m}$, far infrared (FIR) $40-1000\,\mu\mathrm{m}$, and microwaves $1\,\mathrm{mm}-30\,\mathrm{cm}$. These ranges were extracted from selected entries of Meyers (1992) with emphasis on atmospheric aspects. The spectral divisons are not consistent in literature, in particular concerning the infrared and microwaves region. Given ranges therefore have to be taken as approximate values.

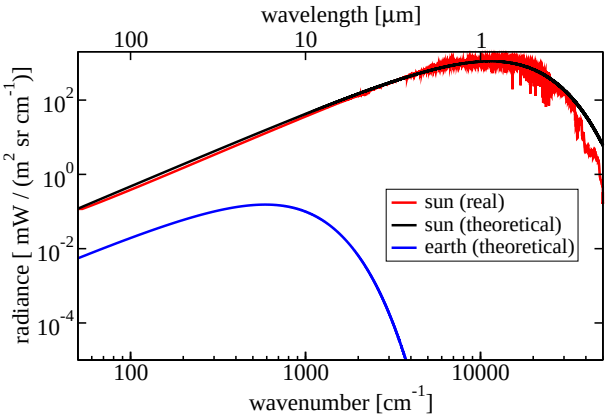

Figure 2.1: *Spectral distribution of solar and terrestrial radiation. Planck blackbody emission for $T = 5800\,K$ (black) and $T = 300\,K$ (blue) as example of theoretical solar and terrestrial radiation on top of atmosphere. A realistic spectrum (Anderson et al., 1995) of incident solar direct beam intensity is plotted for comparison.*

from Kirchhoff's law it can be found that thermal emission is strong in case of high absorption and low in atmospheric windows. Scattering of longwave radiation plays a minor role as will be described in subsection 2.3.2. Nevertheless, in atmospheric windows with low absorption, e.g. between 8 and 12 μm, scattering may not be neglected in general. Significant spectral features in IR and microwave spectra due to scattering can be found in presence of water droplets and ice crystals. In relation to the intensity of solar radiation, which is highly dependent on the relative position of sun and observer, terrestrial radiation in horizontally homogeneous atmospheres is azimuthally independent. Since emission of radiation according to Planck's function is isotropic, anisotropy of the thermal radiation field mainly results from the vertical structure of the atmosphere and temperature layering, in particular.

In conclusion, when modeling radiative transfer in the visible and near infrared region of the spectrum, thermal emission source term J_B is neglected. For far infrared and microwave wavelengths commonly only J_B is included. However, all source terms should be considered between about 2.5 μm and 4 μm, where contributions from solar and terrestrial radiation have the same order of magnitude.

2.3 Radiative Properties of Matter

Until now only interaction of radiation with matter in general has been introduced. In atmospheric radiative transfer matter is usually represented by the atmosphere itself with the planet's surface as a lower boundary and a completely transparent upper boundary. The atmosphere is mainly composed of different gases, but also contains aerosols – small solid particles of diverse chemical composition – as well as hygrosols – fluid droplets or frozen crystals, the basic particles clouds are formed of. While radiation may be transmitted through the atmosphere, the surface as lower boundary absorbs, emits, or reflects radiation, but is usually not considered to transmit radiation. In atmospheric science the soil – possibly covered by vegetation, snow, or ice – or a water surface represent the lower boundary. In the following sections the specific types of matter and their properties with respect to radiation are described.

2.3.1 Molecular Absorption and Scattering

Emission and absorption are processes of exchange of energy between electromagnetic waves and matter. The spectral position, here expressed in terms of wavenumber ν, where emission or absorption occurs, is related to the energy transported by the emitted/absorbed photon via Planck's law of radiation by $E = hc\nu$, where h denotes Planck's constant and c is the speed of light. The energy of a molecule is determined by the sum of its translational, rotational, vibrational and electric energy: $E = E_\mathrm{t} + E_\mathrm{r} + E_\mathrm{v} + E_\mathrm{e}$, with $E_\mathrm{r} < E_\mathrm{t} < E_\mathrm{v} < E_\mathrm{e}$.

Except for translational energy, these energies are quantized and can only take on discrete values. Allowed energy states are well defined but depend on the structure of the particular molecule. Rotational energy changes are small, causing pure rotational spectra in the far infrared and microwave region between approximately $1\,\mathrm{cm}^{-1}$ and several $100\,\mathrm{cm}^{-1}$. Vibrational lines occur from far to near infrared in the region of about $600-10000\,\mathrm{cm}^{-1}$. Electronic transitions lead to radiative activities in the ultraviolet and visible region of the electromagnetic spectrum. Electronic and vibrational transistions usually occur in combination with rotational transistions, forming band structures around the genuine transition frequency of the electronic and vibrational lines.

The position of a spectral line is determined by the amount of energy change when transitions occur. However, emission and absorption due to a single change of energy state is practically never monochromatic, but a spectral line is broadened over a certain wavenumber range. This line broadening is caused by the finite natural lifetime of the energy state (natural broadening), collision between molecules (pressure or collision broadening), and the Doppler effect due to thermal motion of molecules in space (Doppler broadening).

In general, the shape of a line is given by

$$\sigma_\mathrm{a}(\nu) \;=\; S(T)\, F(\nu, T, p), \tag{2.15}$$

where $\sigma_\mathrm{a}(\nu)$ denotes the absorption cross section, $S(T)$ is the line strength and $F(\nu, T, p)$ the line shape function. Line strength, defined as integral of monochromatic absorption cross sections caused by a single line over the whole spectrum, is a specific characteristic of the individual line. Line strength depends on temperature T but is independent of pressure p and is tabulated in spectroscopic line catalogs at a reference temperature T_0. The conversion to other temperatures is usually done according to

$$S(T) \;=\; S(T_0)\, \frac{Q(T_0)}{Q(T)}\, \frac{e^{-E_\mathrm{l}/kT}}{e^{-E_\mathrm{l}/kT_0}}\, \frac{(1 - e^{hc\nu_0/kT})}{(1 - e^{hc\nu_0/kT_0})}, \tag{2.16}$$

where E_l is the lower energy level of the states between which the transition occurs, $Q(T)$ is the partition function, and ν_0 is the transition frequency, the spectral position of the line. E_l, ν_0, and information about $Q(T)$ is contained in line catalogs.

An appropriate line shape function has to be chosen according to the broadening effects that have to be considered. Pressure broadening can be described by the Lorentz profile with line shape function

$$F_\mathrm{L}(\nu, \nu_0) \;=\; \frac{\alpha_\mathrm{L}/\pi}{(\nu - \nu_0)^2 + \alpha_\mathrm{L}^2}, \tag{2.17}$$

where α_L denotes the Lorentzian half width. The dependence of Lorentzian half width α_L on temperature and pressure is approximately given by

$$\alpha_\mathrm{L} \;=\; \alpha_0\, \frac{p}{p_0}\, \left(\frac{T_0}{T}\right)^n, \tag{2.18}$$

where α_0 is the half-width at reference pressure p_0 and reference temperature T_0. Index n depends on the type of the molecule. Reference half-width α_0 and index n are tabulated in spectroscopic databases. Self broadening is neglected in (2.18).

Doppler broadening corresponds to a Gaussian line shape with

$$F_{\mathrm{D}}(\nu,\nu_0) \;=\; \frac{1}{\alpha_{\mathrm{D}}\sqrt{\pi}}\;\exp\left[-\left(\frac{\nu-\nu_0}{\alpha_{\mathrm{D}}}\right)^2\right], \tag{2.19}$$

where α_{D} is the Doppler width of the line given by

$$\alpha_{\mathrm{D}} \;=\; \nu_0\,\sqrt{\frac{2kT}{mc^2}}, \tag{2.20}$$

with m denoting the mass of the molecule. Considering pressure and Doppler broadening simultaneously leads to a Voigt line shape resulting from the convolution of Lorentz and Doppler profiles:

$$\begin{aligned} F_{\mathrm{V}}(\nu,\nu_0) \;&=\; F_{\mathrm{L}}\otimes F_{\mathrm{D}} \;=\; \int_{-\infty}^{\infty} F_{\mathrm{L}}(\nu',\nu_0)\,F_{\mathrm{D}}(\nu,\nu')\,\mathrm{d}\nu' \\ &=\; \frac{1}{\alpha_{\mathrm{D}}\sqrt{\pi}}\,K(x,y) \qquad\qquad \text{and} \qquad (2.21)\\ K(x,y) \;&=\; \frac{y}{\pi}\int_{-\infty}^{\infty}\frac{e^{-t^2}}{y^2+(x-t)^2}\,\mathrm{d}t \qquad (2.22) \end{aligned}$$

where $K(x,y)$ is called the Voigt function and parameters are defined as $x=(\nu-\nu_0)/\alpha_{\mathrm{D}}$ and $y=\alpha_{\mathrm{L}}/\alpha_{\mathrm{D}}$ with interpretation of t as $t=(\nu-\nu')/\alpha_{\mathrm{D}}$.

Natural broadening is negligible compared to the other broadening mechanisms. Basically, the higher the pressure is, the more important is pressure broadening. In the Earth's atmosphere collision broadening prevails below 20 km, while in the upper atmosphere Doppler broadening is dominant. In between about 20 to 50 km altitude – according to Eq. (2.20) depending on the spectral region – the effective line shape is influenced by both pressure and Doppler broadening.

Parameters characterizing the individual transitions of molecules are tabulated in spectroscopic databases like HITRAN (Rothman et al., 2005). These spectroscopic absorption line parameters may be calculated from the theory of quantum mechanics. However, analysis of laboratory data is preferred in practice to derive absorption cross sections or line parameters, especially for complex structured molecules.

Spectral absorption coefficients of mixed media are finally obtained by summing up contributing cross sections from individual lines related to different molecules:

$$\beta_{\mathrm{a}}(\nu) \;=\; \sum_m \left(n_m \sum_l \sigma_{m,l}(\nu) + \beta_m^{\mathrm{ac}}(\nu)\right) \tag{2.23}$$

where $\sigma_{m,l}$ is the absorption cross section of a single line l of molecule m. n_m denotes the number density and β_m^{ac} is the continuum absorption coefficient of molecule m. Continuum absorption, that varies slowly with wavenumber, has been suggested to result from accumulated absorption in the far wings of strong lines, e.g. from water vapor. A rigorous theoretical derivation of absorption continua is still missing, but continuum information has been empirically derived and tabulated, e.g. by Clough et al. (1989) and Liebe (1989).

Exact calculations of absorption spectra from spectral line data can be done with the help of line-by-line (LbL) models, that determine monochromatic absorption cross sections along the profile of individual lines. To represent the line shape correctly, a large number of spectral grid points has to be considered.[3] Since these calculations have to be carried out for individual molecules and several combinations of pressure and temperature, the computational effort is tremendous. Diverse methods have been developed to reduce the effort, for example lower resolution band models (e.g. Elsasser and Culbertson, 1960; Malkmus, 1967) and transmission fitting functions like exponential sum fitting (e.g. Wiscombe and Evans, 1977) and k-distributions (e.g. Lacis and Oinas, 1991; Bennartz and Fischer, 2000). However, the interpretation of high resolution spectral measurements, as performed by Fourier transform spectrometers, require the use of LbL-models.

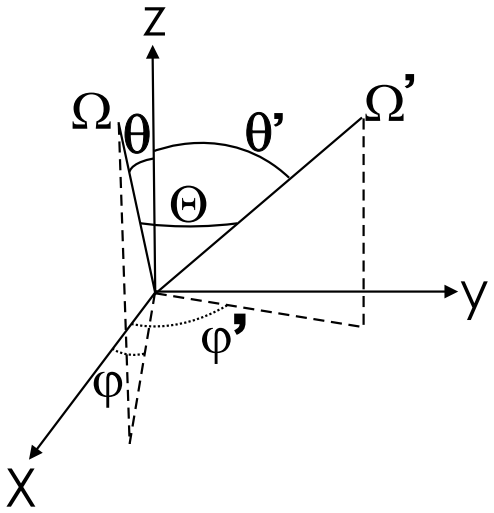

Figure 2.2: *Relation between incident and scattering directions* $\mathbf{\Omega'}$ *and* $\mathbf{\Omega}$ *expressed in terms of zenith* (θ', θ) *and azimuthal angles* (ϕ', ϕ). Θ *denotes the scattering angle.*

In contrast to molecular absorption, spectral dependency of molecular or Rayleigh scattering cross sections is rather smooth:

$$\sigma_{\mathrm{s}}(\lambda) \;=\; \frac{128\pi^5}{3\lambda^4}\;\alpha^2. \tag{2.24}$$

Polarizability α is described in terms of complex refractive index m and total number of molecules in a unit volumne. The Rayleigh phase function is given by

$$P(\Theta) \;=\; \frac{3}{4}\,(1+\cos^2\Theta), \tag{2.25}$$

where Θ denotes the scattering angle, the angle between the directions of incident and scattered radiation, $\mathbf{\Omega'}$ and $\mathbf{\Omega}$, respectively, in the plane of scattering (see Fig. 2.2). In terms of zenith and azimuthal angles the scattering angle is given by

$$\cos\Theta \;=\; \mathbf{\Omega'}\cdot\mathbf{\Omega} \;=\; \cos\theta'\cos\theta + \sin\theta'\sin\theta\cos(\phi'-\phi), \tag{2.26}$$

[3] Assuming the line shape to be represented accurately by resolving the half-width of the line by about four sample points. Then, for typical stratospheric half-widths of $\approx 0.001\,\mathrm{cm}^{-1}$, 40000 spectral grid points are required to cover a spectral range of only $10\,\mathrm{cm}^{-1}$.

with θ and θ' denoting the zenith angle components and ϕ and ϕ' the azimuthal components of incident and scattering directions. The scattering pattern caused by Rayleigh scattering is symmetric in the forward and backward hemispheres and exhibits a minimum at a scattering angle of 90°.

Rayleigh scattering, modeled by Eqs. (2.24) and (2.25) assumes scattering particles to be very small, spherical and isotropic with refractive index close to 1. These assumptions are valid for gaseous matter in the atmosphere, although a correction considering the anisotropic property of molecules is recommended. From Eq. (2.24) with wavelength dependency of λ^{-4} it becomes clear, that Rayleigh scattering due to air molecules is important in the ultraviolet and visible region of the spectrum but negligible at infrared and microwave wavelengths.

2.3.2 Particle Scattering and Absorption

Besides gaseous constituents, atmospheres contain suspended matter, i.e. aerosols, and hygrosols. In contrast to gas absorption explained by the theory of quantum mechanics, scattering and absorption of aerosols and hygrosols can be better understood in terms of classical electrodynamics. Absorption and scattering properties of particulate matter can be described in terms of size parameter x and complex refractive index $m = m_\mathrm{r} - i\, m_\mathrm{i}$. The real part m_r of the refractive index is a measure of the scattering behavior while the imaginary part m_i represents the importance of absorption. The size parameter x, that relates particle size to wavelength of the incident radiation, is defined by

$$x \;=\; \frac{2\pi a}{\lambda}, \tag{2.27}$$

where a denotes the geometrical size of the particle, e.g. the radius r of a sphere. Rayleigh scattering is applicable for particles with $x \ll 1$. For spherical particles with $x \gtrsim 1$, Mie theory – sometimes also referred to as Lorentz-Mie or Mie-Debye theory – has been established, while optical properties of particles with $x \gg 1$ may be calculated with the help of geometric optics.

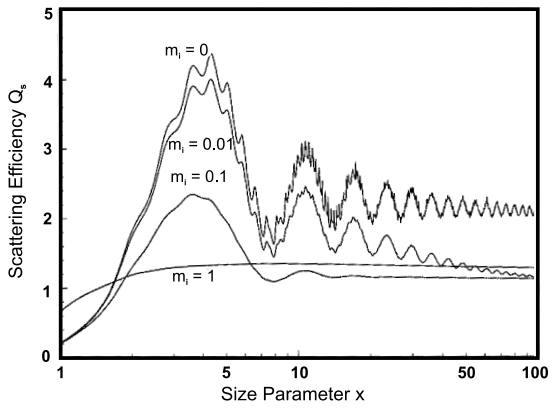

Figure 2.3: *Scattering efficiency as a function of size parameter, derived from Mie theory for a real part of the refractive index $m_r = 1.5$ and an imaginary part m_i as indicated in the plot. Figure adapted from Liou (2002).*

Mie theory describes the optical properties of homogeneous spherical particles by solving the vector wave equation derived from Maxwell's equations. Scattering and extinction efficiency

Q_s and Q_e, respectively, are obtained in terms of complex scattering amplitudes. Absorption efficiency is determined by the principle of energy conservation as

$$Q_\mathrm{a} \;=\; Q_\mathrm{e} - Q_\mathrm{s}. \tag{2.28}$$

Extinction cross section σ_e corresponds to efficiency by

$$Q_\mathrm{e} \;=\; \frac{\sigma_\mathrm{e}}{A} \;=\; \frac{\sigma_\mathrm{e}}{\pi r^2}, \tag{2.29}$$

where A denotes the geometric cross section of an arbitrarily shaped particle. Scattering and absorption cross sections result from scattering and absorption efficiency in an analogous manner. Eqs. (2.28) and (2.29) are generally valid and not restricted to Mie theory. Directional dependency of scattering is given by the phase function $P(\Theta)$, which is derived from the complex scattering amplitudes as well. Θ denotes the scattering angle as introduced in (2.26). While phase function P basically depends on incident and scattering direction explicitly, for spherical particles the angular dependency may be reduced to the scattering angle. This simplification is possible due to the symmetry of the particle, that is represented in the scattering pattern as well.

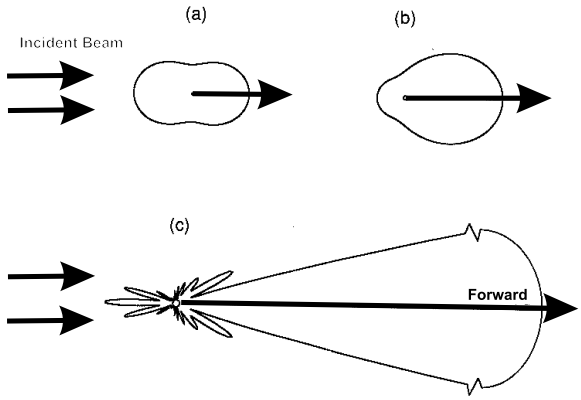

Figure 2.4: *Mie scattering patterns from spherical particles illuminated by light of* $\lambda = 0.5$ μm. *Particles have radii of* 10^{-4} μm *(a), 0.1* μm *(b), and 1* μm *(c). The forward scattering pattern of (c) is extremely large and has been scaled for presentation purposes. Figure adapted from Liou (2002).*

In contrast to Rayleigh scattering, which is proportional to λ^{-4}, Mie scattering is linearly varying with wavelength. Nevertheless it is critically dependent on size parameter and refractive index. With respect to size parameter scattering efficiency shows some major extrema, resulting from interference of light diffracted or transmitted by the particle, and ripple structures which arise from grazing edge rays. Both, major extrema as well as ripple structures become smoother with larger imaginary part of the refractive index, i.e. with increasing importance of absorption (see Fig. 2.3). For large size parameters, scattering efficiency approaches an asymptotic value, which is 2 for non-absorbing particles and between 1 and 2 for absorbing ones.

Mie phase functions show a strong forward peak due to diffraction and a slighter peak in backward direction. The minimum of the phase function, which is at 90° for Rayleigh particles is found at larger scattering angles. When particles become large compared to the wavelength

of incident radiation, rapid fluctuations of the phase function occur due to interference effects (see Fig. 2.4).

In geometric optics, radiation may be thought as a bundle of parallel rays, separately undergoing events of refraction and reflection, transmission and absorption inside and outside the particle with directions of refraction determined by Snell's law. A practical solution for scattering of light by particles of arbitrary size and shape does not exist. Several methods for the determination of optical properties of non-spherical particles have been presented and shown to be advantageous for special cases, e.g. the unified theory for scattering of ice particles by Liou (2002), which combines geometric optics with the so-called finite time domain method, and the T-matrix (Mishchenko et al., 2002) method, that is very efficient for scattering calculations involving rotationally symmetric particles.

The previously described optical properties have been derived for single particles. Realistic atmospheres contain mixtures of particles with various sizes as well as different regimes of particles with respect to chemical components. The size of particles in a polydispersion is commonly described by the particle size distribution $n(a)$, describing the number density, the number of particles per unit volume, with respect to their size a. For different particle regimes different size distributions were developed. The most widely used size distributions are log-normal distributions with the basic form

$$n(a) \;=\; \frac{C}{a\,\sigma_0}\;\exp\left[\frac{-(\log a - \log a_\mathrm{m})^2}{2\sigma_0^2}\right], \tag{2.30}$$

where C is a constant, σ_0 measures the width of the distribution and a_m denotes the modal diameter, and (modified) gamma distributions with the basic form

$$n(a) \;=\; C\,a^\alpha\;\exp(-b\,a^\gamma) \tag{2.31}$$

where C, a, b and γ are parameters defining the distribution. The total number of particles is obtained by

$$N \;=\; \int_{a_\mathrm{min}}^{a_\mathrm{max}} n(a)\,\mathrm{d}a, \tag{2.32}$$

with a_min and a_max being the minimum and maximum particle size considered by the distribution, respectively. Log-normal distributions are usually related to aerosol particles with tabulated distribution width and modal diameter for specific aerosol components (World Climate Research Program, 1986), while gamma distributions are often used for water and ice clouds (e.g. Shettle, 1990).

Scattering by samples of particles is assumed to be independent, i.e. a scattering event at one particle does not interfere with those at other particles. In consequence, scattered intensities may be added without regard to the phases of the individual scattered waves. Thus, bulk optical properties can be obtained by a weighted mean of single particle properties. The extinction coefficient of a sample of particles is given by

$$\beta_\mathrm{e} \;=\; \int_{a_\mathrm{min}}^{a_\mathrm{max}} n(a)\,\sigma_\mathrm{e}(a)\,\mathrm{d}a. \tag{2.33}$$

Scattering as well as absorption coefficients can be calculated analogously. The phase function of a polydispersion is derived from

$$\beta_\mathrm{s}\,P(\Theta) \;=\; \int_{a_\mathrm{min}}^{a_\mathrm{max}} n(a)\,\sigma_\mathrm{s}(a)\,P(\Theta,a)\,\mathrm{d}a. \tag{2.34}$$

The relation of scattering to extinction by a sample of particles is called single scattering albedo and defined as

$$\omega_0 \;=\; \beta_\mathrm{s}/\beta_\mathrm{e}. \tag{2.35}$$

When absorption is negligible, i.e. $\beta_\mathrm{e} \approx \beta_\mathrm{s}$ and $\omega_0 \approx 1$, one speaks of conservative scattering, referring to the conservation of radiative energy.

Beside so-called elastic scattering, where incident and scattered radiation have the same wavelength, wavelength shifts can occur during a scattering event. An example of inelastic scattering, characterized by a change of wavelength, is Raman scattering (Raman, 1928). Within this work only elastic scattering is considered.

2.3.3 Radiative Properties of Surfaces

Beside being dependent on atmospheric conditions, the radiation field in the atmosphere is affected by the presence of a lower boundary, which absorbs and reflects incident radiation and thermally emits radiation. The lower boundary surface can be a land or water surface, or some atmospheric layer acting as "effective surface", e.g. a dense cloud layer. Radiative properties of the surface primarily depend on the material, its chemical composition, roughness, and texture.

Basically, the variation of absorption and reflection properties with wavelength is smooth, characterized by spectral band features, or resembles a continuous spectrum. However, at wavelengths close to resonance frequencies, sharp changes in the spectrum may occur. Optical surface properties could be described in terms of refractive index, but due to the wide range of substance mixtures, that occur among natural surfaces, it is common to tabulate their spectral properties for practical reasons.

In contrast to optical properties of atmospheric constituents, equivalent surface properties are defined as dimensionless ratios of absorbed or scattered intensity to incident energy. Ratios may be derived with respect to a certain direction, describing the angular dependency, or to fluxes, presenting the average characteristic of the surface concerning the optical quantity. Absorption and emission of the surface are usually considered to be isotropic, i.e. independent of direction. They are described by the parameters absorptivity α_surf and emissivity $\varepsilon_\mathrm{surf}$ with the latter defined by

$$\varepsilon_\mathrm{surf} \;=\; \frac{I(\Omega)}{B(T_\mathrm{surf})}, \tag{2.36}$$

where Ω denotes the direction of emission into the upper hemisphere and T_surf is the temperature of the surface. In case of local thermodynamic equilibrium absorptivity is equal to emissivity according to Kirchhoff's law.

When considering no transmission through the surface, from the principle of energy conservation follows

$$\alpha_\mathrm{surf} + r_\mathrm{surf} \;=\; \varepsilon_\mathrm{surf} + r_\mathrm{surf} \;=\; 1, \tag{2.37}$$

where r_surf denotes the reflectivity or albedo of a surface. The albedo is defined as ratio of the flux of radiation, reflected back into the upper hemisphere, to the incident radiation from a certain direction:

$$r_\mathrm{surf} \;=\; \rho(2\pi, -\Omega') \;=\; \frac{\int_0^{2\pi} I(\Omega)\cos\theta\,\mathrm{d}\Omega}{I(-\Omega')\,\cos\theta'}, \tag{2.38}$$

where Ω' is the incident direction of downwelling radiation and θ' its zenith angle component. Generally, reflection varies with both, direction of incidence and reflection. These dependencies

are described by the bidirectional reflection distribution function (BRDF), giving the ratio of reflected intensity to the energy incident to a surface element from a certain direction for all combinations of incident and reflection direction, Ω' and Ω:

$$\rho(\Omega, -\Omega') \;=\; \frac{I(\Omega)}{I(-\Omega')\,\cos\theta'}. \tag{2.39}$$

Specular and diffuse reflection may be distinguished. Specular reflection occurs on perfectly smooth surfaces, e.g. calm water or clean ice, where all reflected radiation is directed along the angle of mirror reflection. That means, Eq. (2.39) transforms into a delta-function. Specular reflection from smooth dielectric surfaces, e.g. water, can be calculated from the refractive index of the surface material with the help of Fresnel's equations. Cox and Munk (1954) derived an analytic model for sea-surface reflectance based on Fresnel's equations and probability distributions for orientation of scattering facets of the surface depending on wind speed.

Diffuse reflection denotes reflection of an incident beam into all directions of the upper hemisphere. Diffuse reflection occurs due to microscopically irregular surface structures, presenting a variety of facets with different surface normals to incident radiation. Most surfaces exhibit both, a specular and a diffuse component.

Completely uniform angular distribution of reflection is called Lambertian reflection. Then reflection is independent of direction of incidence and observation and the BRDF reduces to a constant:

$$\rho(\Omega, -\Omega') \;=\; \rho_{\mathrm{L}} \;=\; \text{const.} \tag{2.40}$$

for all Ω' and all Ω.

Similar to scattering by atmospheric particles it can be observed that radiation fields are highly affected by surface reflection in the shortwave spectral region. Emission dominates in thermal infrared and microwave region, where reflection plays only a minor role.

2.4 Composition and Structure of the Earth's Atmosphere

2.4.1 Vertical Structure

The atmosphere is commonly divided into layers according to their thermal state (Fig. 2.5(b)). The lowermost region, the troposphere, is characterized by decreasing temperature with respect to height, which is mainly a consequence of "heating" from the surface. Temperature decreases from a mean temperature of 288 K at the surface to around 220 K with a lapse rate of 6.5 K/km. The troposphere is followed by the stratosphere, where temperature increases due to strong absorption of solar ultraviolet radiation by ozone. Between around 50 – 90 km altitude, in the so-called mesosphere, temperature decreases again. In the thermosphere, above 90 km, temperature ranges up to 2000 K caused by absorption of energetic ultraviolet and X-ray radiation. The assumption of local thermodynamic equilibrium is not valid in the thermosphere.

Vertical structuring may also be observed according to further physical parameters like pressure and density as well as according to chemical composition. Pressure and density are related through the hydrostatic equilibrium. Forced by gravity this leads to an exponential decrease of pressure and air density with height:

$$p(z) \;\approx\; p(z_0)\, e^{-(z-z_0)/H}, \tag{2.41}$$

where H is the scale height, which is $\approx 6-8$ km in the Earth's atmosphere. Horizontal variations usually occur on larger spatial scales. Therefore the atmosphere is customarily taken to be a horizontally homogeneous, slab medium.

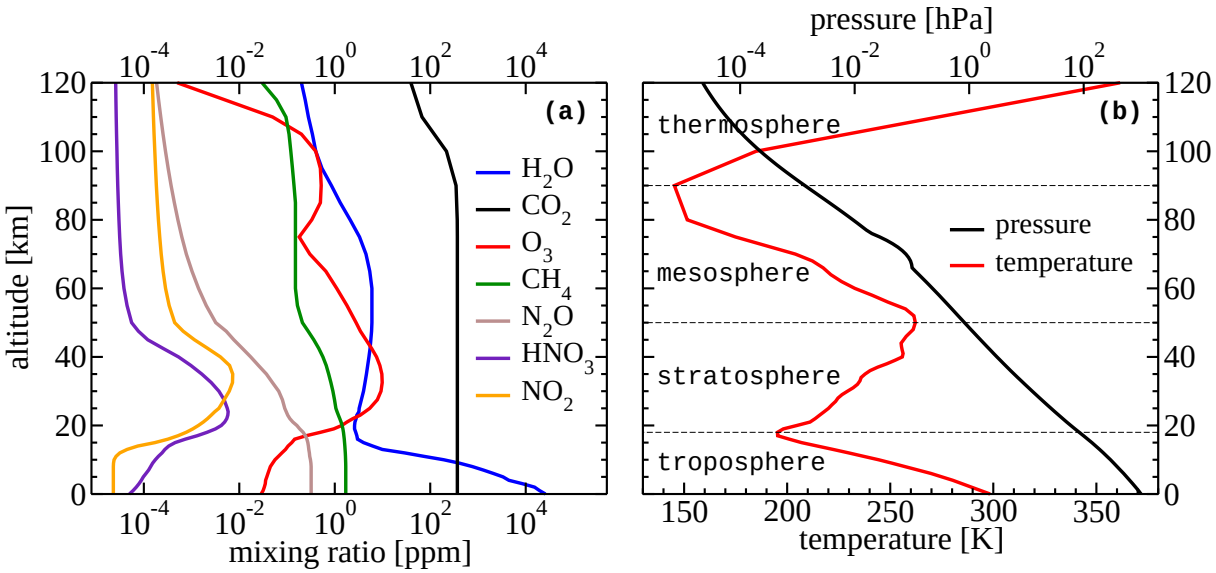

Figure 2.5: *Vertical structure of the Earth's atmosphere. (a) Volume mixing ratio profiles of exemplary molecules of a standard atmosphere. (b) Atmospheric layering according to vertical temperature profile.*

2.4.2 Gaseous Constituents

Air is a mixture of several gaseous species. The standard mixture contains nitrogen (N_2, 78%), oxygen (O_2, 21%) and argon (Ar, 1%), together accounting for about 99,96% of the air's volume. These gases are permanent, well-mixed species, such that partial density and pressure of each species obey Eq. (2.41). This also applies to long-lived minor species like carbon dioxide (CO_2), methane (CH_4), nitrous oxide (N_2O), and a number of inert gases.

Concentrations of other species are variable in space and time due to their forming mechanisms. The most important are water vapor, whose concentration is highly dependent on the ambient temperature and rapidly decreasing with height, and ozone, forming a layer between about 15 to 35 km altitude due to photochemical processes. For species of at least partial anthropogenic origin, such as CO_2, CH_4, N_2O, and NO_x as well as chlorofluorocarbons (CFCs), concentrations are observed to increase continuously. Fig. 2.5(a) shows an example of standard mixing ratios of selected molecules.

Although N_2 and O_2 amount to almost all air by volume, they are generally irrelevant concerning absorption at visible and infrared wavelengths. Minor species and trace gases are of much greater interest concerning radiative processes. Ultraviolet radiation is blocked by the stratospheric ozone layer. That is not only essential for protecting life from highly energetic solar radiation, but is also responsible for the increasing temperatures in the stratosphere mentioned before.

Due to absorption of radiation in several rotational and vibrational-rotational bands, water vapor and carbon dioxide are of key importance to the heat balance of the atmosphere. They allow the transmittance of shortwave radiation to the surface, but strongly absorb infrared radiation, thermally emitted by the surface and the atmosphere itself. This leads to a "trapping" of radiative energy, known as the greenhouse effect. It causes significantly higher temperatures of the Earth's surface and troposphere than would be expected without such gases. Further relevant greenhouse gases are CH_4 and the CFC species, that form extensive bands in the thermal infrared. The spectral behavior of greenhouse gases, causing the atmosphere to be transparent in the visible spectrum and opaque in the infrared except for some atmospheric windows, e.g. between $8\,\mu$m and $12\,\mu$m, motivates the separation of solar and terrestrial radiative transfer as explained in section 2.2.

2.4.3 Aerosols

Horizontal homogeneity does not apply to aerosols and hygrosols in the same way as to gaseous matter. Aerosols tend to have distinct sources, but are spread over huge areas through transport processes. Most of the aerosol particles are released by interaction between the lowest atmospheric layer and the surface. Hence, the planetary boundary layer, which is the lowest 1 km of the troposphere, holds the greatest variety and concentration of particles. Particle number density in the boundary layer decreases rapidly with height. Largest concentrations are observed in urban and desert areas. The stratosphere contains a thin layer of sulfurous particles, known as the Junge layer, usually located between the tropopause and 30 km altitude. At higher altitudes, the atmosphere is virtually free of particles.

Aerosols can be of natural origin, such as volcanic and wind blown dust and sea salt. Others are produced by human activities, e.g. through combustion processes. They are usually classified in terms of their type (e.g. continental, maritime), location (e.g. rural, urban, desert) and particle load (clear, average, polluted). These aerosol classes are mixtures of different individual components, which are grouped into basic categories like soot, sulfate, dustlike particles, water solubles etc. Each basic component is characterized by a certain size distribution and a spectrum of refractive indices, which determine their optical properties. A number of aerosol models have been developed, tabulating the composition of several aerosol classes along with the microphysical properties of their basic components (World Climate Research Program, 1986; d'Almeida et al., 1991).

The size of aerosol particles ranges from $10^{-3}\,\mu$m to about $20\,\mu$m with a majority having sizes in the order of $0.1\,\mu$m. Size distributions may be very complex, but are approximately represented by analytic functions dependent on few parameters like a log-normal distribution. Associated with different formation mechanisms, aerosols are frequently divided into two size classes. Particles with diameters larger than 1 μm are produced through disentanglement from bulk materials and suspension by the wind, e.g. dust and sea salt. Smaller particles are formed by combustion processes or chemical conversion of gaseous matter into liquid and solid products, e.g. soot. Bimodal size distributions are represented by a sum of two single mode size distributions as given in Eqs. (2.30) and (2.31).

Hygroscopic particles interact with ambient water vapor and change their size in dependence on relative humidity. This process may also effect shape as well as chemical composition and consequently optical properties of the aerosol. Furthermore, humidity effects are related to formation of hygrosols with small aerosols acting as condensation and ice nuclei. Aerosol particles

occur with great variety of shapes from quasi-spherical to highly irregular, e.g. in form of clusters and aggregates. However, for simplification they are usually assumed to be spherical and are treated according to Mie theory in radiative transfer modeling.

Radiative properties of aerosols strongly depend on the refractive index of the components as well as on the effective size or size parameter of the mixture. In the visible spectral region, aerosol scattering is dominating. Absorption is small for oceanic and sulfate particles and stronger for mineral, dustlike, and water soluble components. Soot is strongly absorbing from ultraviolet to microwave wavelengths. In the infrared region, size parameters for most of the aerosols become very small. Scattering efficiency rapidly decreases such that absorption becomes dominant. Nevertheless, the absorption efficiency reduces as well, meaning extinction due to aerosols becomes much smaller and often even negligible in the infrared.

2.4.4 Clouds

Clouds regularly cover more than 50% of the sky, but cloud occurence is highly variable in space and time. Various types of clouds may be distinguished with respect to altitude, cloud phase (liquid water or ice), particle concentration, size, and shape. Conventionally they are classified in terms of position and visual appearance. Low clouds with base heights lower than 2 km are generally composed of water droplets. Their sizes range from about 1 μm to 20 μm with a typical size of 5 μm. Except for very large droplets, they are of spherical shape.

Cirrus clouds are found from the upper troposphere to the lower stratosphere and are exclusively composed of nonspherical ice crystals. Crystal size and shape primarily depend on temperature and humidity. The lower temperature and humidity are, the smaller and more pristine crystals – hollow and solid columns, plates and needles – are formed. At higher temperature, approximately around -40° C, and larger humidity spatial crystals like rosettes and clusters predominate. At the bottom of cirrus clouds highly irregular particles like aggregates are produced by collision due to vertical mixing and gravitational attraction.

Ice crystals may reach sizes $> 1000\,\mu$m, but have typical effective sizes of $20\,\mu\text{m} - 100\,\mu$m. Thin cirrus, that is occasionally subvisible, primarily contains small crystals between 5 μm and 20 μm. Because of great variability in space and time and due to different atmospheric conditions, representative values of ice crystal size and shape are difficult to derive. On the basis of a number of intensive field observations during the last decades (e.g. Cox et al., 1987; Raschke et al., 1990; Heymsfield et al., 1998), "typical" microphysical properties were retrieved and parameterizations have been empirically developed for midlatitude (Heymsfield and Platt, 1984; Sassen and Benson, 2001) and tropical cirrus (McFarquhar and Heymsfield, 1997; Guo et al., 2005).

In polar regions so-called polar stratospheric clouds (PSC) occur during the polar night period in altitudes between 20 and 30 km, where temperatures are lower than -80° C. In contrast to cirrus they consist of small, nearly spherical ice particles mainly composed of nitric acid and water.

Clouds at mid-altitudes usually contain both water droplets and ice particles, the former dominating the lower parts, the latter predominantly occurring at cloud tops. At temperatures between 0° C and -20° C, supercooled water droplets coexist with ice particles. Ice and water have different refractive indices. Furthermore, ice particles tend to be larger than water droplets. Thus, optical and radiative properties of mixed phase clouds clearly differ from pure water as well as from pure ice clouds. Yang et al. (2003) have shown, that even minor amounts of small water droplets lead to significantly different spectral signatures, especially in the atmospheric window between 8 μm and 12 μm.

Water clouds use to be opaque from the UV to the FIR spectral region, but become transparent in the microwave spectral region. Shortwave radiation is primarily scattered, while water clouds act nearly like blackbody radiators at infrared wavelengths.

Cirrus clouds are highly reflecting in the visible spectrum and usually transparent in the thermal infrared, particularly in the atmospheric windows around 3.7 μm and 10 μm. Consequently they can not be treated as blackbodies in radiative transfer with exception of ice clouds, that contain very large crystals. The effect of cirrus clouds on emission spectra varies strongly depending on observation direction and cloud optical depth. At nadir directions observed signals decrease over the entire infrared spectrum since radiation emitted by the warm surface is attenuated. In the 10 μm window, spectral features can be observed that are associated with the ice absorption band centered around $\approx$ 12 μm.

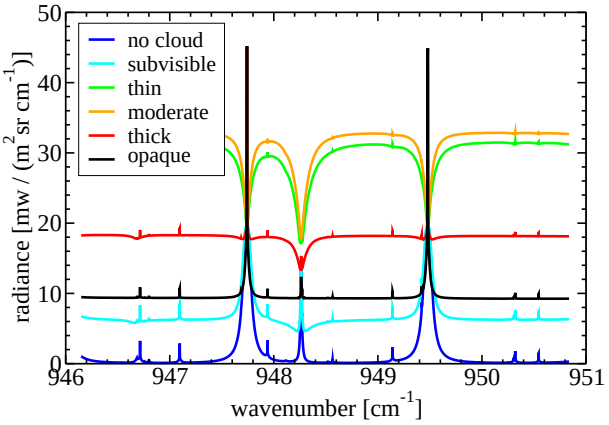

Figure 2.6: *Effect of PSC-type ice clouds of diverse optical thickness on limb emission spectra.*

For limb observations, signals can increase as well as decrease compared to cloud free measurements. Decreasing occurs in spectral regions and at tangent altitudes, that are dominated by gaseous absorption. In the window regions, where only small continuum signals are observed in cloud free cases, radiation increases and may reach significantly higher intensities than a blackbody of cloud temperature would emit (Höpfner and Emde, 2005). While in clear-sky cases only the signal of the relatively cold and thin upper atmosphere is observed, radiation emitted by the warmer lower atmospheric layers and especially the surface is scattered into the limb line of sight. Furthermore, radiation emitted by the cloud contributes to the continuum signal. Maximum radiation enhancements occur when the cloud is vertically transparent, and therefore all layers of the cloud are illuminated by terrestrial radiation, but opaque in limb. When the cloud becomes optically thicker, the radiance reduces again to a value of or below blackbody radiation (see Fig. 2.6).

For thin and subvisible cirrus clouds, observed limb spectra possess spectral features, e.g. broad H_2O and CH_4 absorption lines, that can only be caused by interaction of the radiation with lowest atmospheric layers. Limb observations of the stratosphere and upper troposphere are commonly emission spectra. Furthermore, the limb lines of sight do usually not penetrate the deep layers of the atmosphere, where concentration of water vapor and methane is large and pressure is high enough to cause broad line features. The effect of broad absorption lines in limb spectra is caused by scattering of radiation into the line of sight, that has been emitted by the warm surface and lowest parts of the troposphere and transmitted through the lower troposphere,

where strong absorption occurs in H_2O and also CH_4 lines. Therefore, the transmitted radiation shows tropospheric spectral features, that are overlaid to the upper tropospheric and statospheric limb emission spectra.

Those features are missing when the cloud is optically thick. In that case, surface radiation is attenuated by the lower fractions of the cloud and does not penetrate to the cloud top anymore. For opaque clouds emission from the cloud itself dominates, which is of spectral broadband behavior (see Fig. 2.6). In chapters 4 and 6 effects of ice clouds on thermal infrared limb emission spectra will be examined in detail. The need and advantages of accounting for processes caused by cirrus clouds in order to allow interpretation of observed cloud "contaminated" spectra will be presented.

2.4.5 The Surface of the Earth

Properties of surfaces are related to the material of the soil, surface roughness, moisture, surface cover like vegetation or snow, etc. Emissivity, reflectivity, and reflection function vary greatly from surface to surface in the visible spectral region. At infrared wavelengths most surfaces are good emitters with emissivity $\varepsilon_{\text{surf}} > 0.95$. This strong absorption in the infrared allows to treat them as blackbodies. Nevertheless, some surface types like sand have distinct spectral features that should not be neglected in radiative transfer. Fig. 2.7 presents some examples of optical properties of common surfaces.

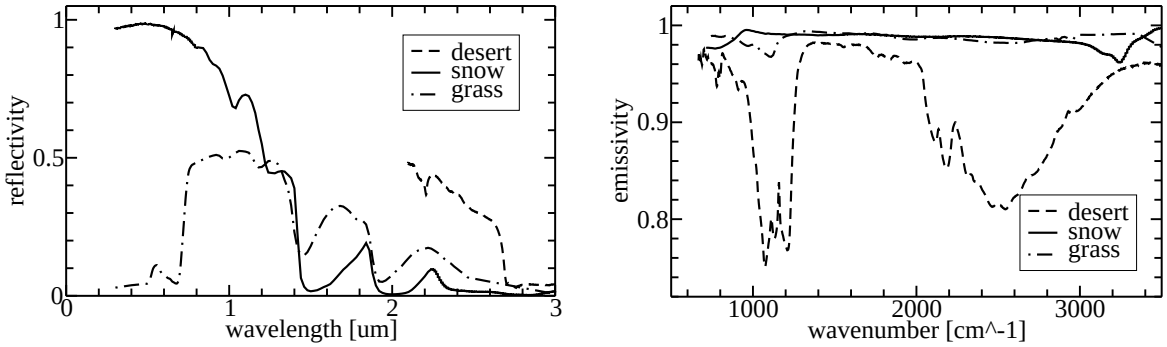

Figure 2.7: *Optical properties of desert soil, medium coarse snow and green grass in the shortwave and longwave spectral region, respectively. Reproduced from the ASTER Spectral Library through the courtesy of the Jet Propulsion Laboratory, California Institute of Technology, Pasadena, California. ©1999, California Institute of Technology. ALL RIGHTS RESERVED. (Hook, 2005)*